RSC Advances

This is an *Accepted Manuscript*, which has been through the Royal Society of Chemistry peer review process and has been accepted for publication.

Accepted Manuscripts are published online shortly after acceptance, before technical editing, formatting and proof reading. Using this free service, authors can make their results available to the community, in citable form, before we publish the edited article. This *Accepted Manuscript* will be replaced by the edited, formatted and paginated article as soon as this is available.

You can find more information about *Accepted Manuscripts* in the Information for Authors.

Please note that technical editing may introduce minor changes to the text and/or graphics, which may alter content. The journal's standard Terms & Conditions and the Ethical guidelines still apply. In no event shall the Royal Society of Chemistry be held responsible for any errors or omissions in this *Accepted Manuscript* or any consequences arising from the use of any information it contains.

ROYAL SOCIETY OF CHEMISTRY

www.rsc.org/advances

Cite this: DOI: 10.1039/c0xx00000x

www.rsc.org/xxxxxx

ARTICLE TYPE

An efficient photocatalyst used in a continuous flow system for hydrogen evolution from water: TiO_2 nanotubes arrays fabricated on Ti meshes

Ruixue Zhou,[a] Shi-Zhao Kang,*[,a] Xiangqing Li,[a] Lei Wang,[b] Lixia Qin,[a] and Jin Mu*[,a]

Received (in XXX, XXX) Xth XXXXXXXXX 20XX, Accepted Xth XXXXXXXXX 20XX

DOI: 10.1039/b000000x

Abstract

In the present work, TiO_2 nanotubes arrays were fabricated on metallic Ti meshes using anodic oxidation method, and decorated with Pt via electrodeposition. Meanwhile, the application of the TiO_2 nanotubes arrays loaded with Pt in a continuous flow system was explored as a photocatalyst for H_2 evolution from water. Furthermore, for practical purposes, the photocatalytic H_2 evolution was studied as a function of content of loaded Pt, annealing temperature, anodic oxidation time, and flow velocity, respectively. The results indicate that the TiO_2 nanotubes arrays fabricated on metallic Ti meshes are an efficient photocatalyst which can be used in a continuous flow system for H_2 evolution from water. During the first hour of irradiation, a rate of H_2 evolution of approximate 4.6 L m^{-2} h^{-1} was achieved under optimal conditions. Moreover, the photocatalytic activity of the TiO_2 nanotubes arrays fabricated on Ti meshes is obviously higher than that of the TiO_2 nanotubes arrays fabricated on metallic Ti foils. The rate of H_2 evolution can increase by a factor of 5 when the TiO_2 nanotubes arrays are fabricated on metallic Ti meshes. Finally, the photocatalytic mechanism was preliminarily discussed.

1. Introduction

Photocatalytic hydrogen evolution offers a valuable way to overcome energy source and environment challenges.[1-3] A lot of efforts have been devoted to develop a stable and efficient photocatalyst since 1972. Therein, nanostructured TiO_2 has been one of the most attractive subjects due to excellent physicochemical properties, low cost and low toxicity.[4-8] Numerous high-efficiency TiO_2-based nanophotocatalysts, such as nanoparticles,[9] nanofibers,[10] nanowires,[11] nanotubes,[12] nanorods[13] etc, have been reported and exhibited good prospects in the field of photocatalytic hydrogen evolution. However, there are still a few practical problems needing to be solved before the commercialization of TiO_2-based nanophotocatalyst becomes possible: (a) separation of the catalyst from the suspension is difficult; (b) the nanostructured TiO_2 tends to aggregate and (c) suspensions are difficult to be applied to continuous flow systems.[14]

Nowadays, various attempts have been made to overcome these problems above. Among the methods reported previously, immobilization of TiO_2 nanoparticles on solid substrates is regarded as an effective and promising way due to simplicity and convenience. However, the TiO_2 nanoparticles immobilized on solid substrates often demonstrate a small surface area. In addition, chaotic structures and grain boundaries will be unfavorable to the photon-generated carriers transfer. As a result, the photocatalytic hydrogen evolution over the immobilized TiO_2 nanoparticles is always unsatisfactory. Compared with the immobilized TiO_2 nanoparticles, the TiO_2 nanotubes arrays fabricated on solid substrates possesses much larger specific surface area, much higher aspect ratio and orientated structure, suggesting that design and fabrication of TiO_2 nanotubes arrays may be a more attractive and essential topic in the photocatalytic hydrogen evolution.

More recently, the TiO_2 nanotubes arrays have been fabricated on various substrates including Ti foils[15] and Ti meshes[16] etc, and their applications in the fields of photocatalysis,[17] solar cell,[18] and photoelectrochemical hydrogen generation[19] begin to attract widespread research interest. As expected, the TiO_2 nanotubes arrays fabricated on solid substrates display many attractive features when used as a photoelectrode in photoelectrochemical hydrogen generation.[20-25] Particularly, compared with the TiO_2 nanotubes arrays fabricated on titanium foils, the TiO_2 nanotubes arrays fabricated on Ti meshes exhibit more noteworthy properties, such as larger specific surface area, 3-D hierarchical nanostructure, flexibility, and low efficiency-dependence on the angle of incident light and so on. Thus, it can be expected that many opportunities may be found in the field of solar energy-to-hydrogen conversion using the TiO_2 nanotubes arrays fabricated on Ti meshes.[26] However, in the case of the TiO_2 nanotubes arrays fabricated on Ti meshes, most of the studies were focused on the application in solar cell and photoelectrochemical hydrogen generation. To our best knowledge, there is no paper on the application of the TiO_2 nanotubes arrays fabricated on Ti meshes as a catalyst for the photocatalytic hydrogen evolution

RSC Advances Accepted Manuscript

from water so far.

The TiO_2 nanotubes arrays fabricated on Ti meshes possess large specific surface area, high aspect ratio and 3-D hierarchical nanostructure, which are favorable to the photon-generated carriers transfer and light harvest. Not only can the metallic reticular backbones serve as stable and flexible supporting substrates, but also offer more convenience for the design of reactors when the TiO_2 nanotubes arrays fabricated on Ti meshes are used in a continuous flow photocatalytic system. Therefore, it can be deduced that the TiO_2 nanotubes arrays fabricated on Ti meshes may be a promising candidate for photocatalytic H_2 evolution in a continuous flow system. Following this idea, the TiO_2 nanotubes arrays were fabricated on Ti meshes (TTA-m) using anodization technique and decorated with Pt via electrodeposition. And the photocatalytic activity of TTA-m loaded with Pt was explored systematically for the photocatalytic H_2 production in a continuous flow photocatalytic apparatus using triethanolamine as a sacrificial agent. Finally, the photocatalytic mechanism was preliminarily discussed.

2. Experimental

2.1. Materials

All chemical reagents were commercial available and used without further purification. Ammonium fluoride (AR) and acetone (AR) were purchased from Shanghai Titanchem Co. Ltd (China). Ethanol (AR), ethylene glycol (AR), hydrochloric acid (AR), sodium hydroxide (AR), hexachloroplatinic acid (AR), triethanolamine (AR) and tetrabutyl titanate (CP) were purchased from Sinopharm Chemical Reagent Co. Ltd (China). The commercial TiO_2 nanoparticles (P25) were supplied by Degussa Co. Ltd (Germany). All solutions were prepared using deionized water as a solvent.

2.2. Fabrication and decoration of TiO_2 nanotubes arrays

The TiO_2 nanotubes arrays were fabricated on Ti meshes according to the procedure similar to one reported previously.[27] The decoration of the TiO_2 nanotubes arrays was carried out following the reported process.[28] (1) A piece of Ti mesh (3.7 cm×3.4 cm, 60 mesh, wire diameter 0.1 mm) was rinsed ultrasonically with water, ethanol and acetone, respectively. After washed with deionized water, the Ti mesh was dried at room temperature in air. Then, the edges of the Ti mesh were packaged using epoxy resin to prepare the work electrode. The bare area of the Ti mesh is 3 cm×3 cm. (2) The two-step anodizing process was performed using a DC power source (Agilent E3643A, Agilent Technologies Inc., USA) in a homemade two-electrode cell. The packaged Ti mesh and the platinum electrode were used as the work electrode and the counter electrode, respectively. The electrolytes used were ethylene glycol containing NH_4F (0.65 wt %) and H_2O (2 vol.%). The Ti mesh was first anodized at 60 V for 30 min, and then treated ultrasonically for 15 min in deionized water. Next, the Ti mesh was anodized continuously at 20 V for 30 min, then 25 V for 30 min, and finally 30 V for 30 min. (3) The decoration of TTA-m was performed using a CHI660D electrochemical system (Shanghai Chenhua Instruments, China) in a conventional three-electrode cell containing H_2PtCl_6 aqueous solution (10 mmol·L^{-1}). The working electrode was TTA-m prepared freshly. An Ag/AgCl electrode and a platinum electrode were used as the reference electrode and the counter electrode, respectively. Cyclic voltammetry was carried out from -0.4 to 0.5 V at a scan rate of 0.01 V·s^{-1}. (4) TTA-m modified with Pt was annealed at 450 °C under ambient air for 1 h. The heating rate is 5 °C·min^{-1}. The amount of Pt deposited is calculated according to equation 1.

$$\text{Content of Pt} = Q/(F\times n\times S) \quad (1)$$

Where Q is the total electric quantity passed through the electrode, F is Faraday constant (96485 C·mol^{-1}), n is the number of electrons transferred in electrochemical reaction, and S is the specific surface area of TTA-m.

2.3. Characterization

Crystal structure identification of the sample was carried out using a PAN analytical Xpert Pro MRD X-ray diffractometer (Netherlands). The scanning electron microscope (SEM) image and the field emission scanning electron microscope (FESEM) images were taken with a Hitachi S-3400N (Japan), and a Hitachi SU8010 (Japan), respectively. The transmission electron microscope (TEM) images and the high resolution transmission electron microscope (HRTEM) image were taken with a JEOL JEM-2100F transmission electron microscope (Japan). X-ray photoelectron spectroscopy (XPS) analysis was carried out on a Thermo Fisher ESCALAB 250Xi X-ray photoelectron spectrometer (USA). The N_2 adsorption and desorption isotherm was measured on a Micromeritics ASAP 2020 nitrogen adsorption apparatus (USA). UV-visible spectra were recorded on a Hitachi U3900 UV-Vis spectrophotometer (Japan).

2.4. Photocatalytic activity test

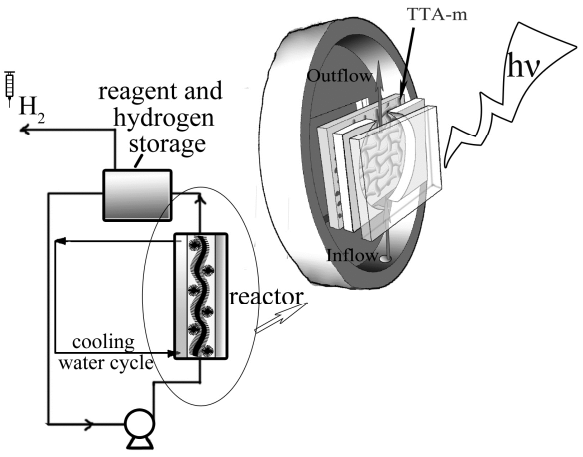

Scheme 1 Schematic diagram of the home-made photocatalytic continuous flow system.

The photocatalytic reaction was carried out in a gas-closed continuous flow apparatus with a homemade reactor (Scheme 1). A 500 W high pressure Hg lamp equipped with an optical filter (λ

RSC Advances Accepted Manuscript

This journal is © The Royal Society of Chemistry [year]

< 420 nm) to cut off the light in the visible region was used as a light source. The distance between the lamp and the reactor is 3 cm. In a typical process, a piece of TTA-m (3 cm×3 cm) was put into the homemade reactor. After sealed, the reactor was connected with a pump and a gas-closed vessel containing tri-ethanolamine aqueous solution (100 mL, 1 mol·L^{-1}). Then, the air was expelled from the reactor by pumping the tri-ethanolamine aqueous solution into the reactor. Consequently, N_2 was bubbled into the tri-ethanolamine solution for 30 min along with pumping. Finally, the pumping rate of tri-ethanolamine aqueous solution was adjusted to be 25 mL·min^{-1}, and then TTA-m was irradiated. After a certain period of irradiation, the amount of hydrogen produced was measured with a gas chromatograph (GC-7900, China, molecular sieve 5A, TCD) using N_2 as a carrier gas The H_2 evolution rate is calculated according to equation 2.

$$H_2 \text{ evolution rate} = \text{the amount of } H_2 /(t \times A) \quad (2)$$

Where t is the irradiation time and A is the irradiated area of Ti mesh when the mesh is assumed to be a solid sheet.

3. Results and discussion

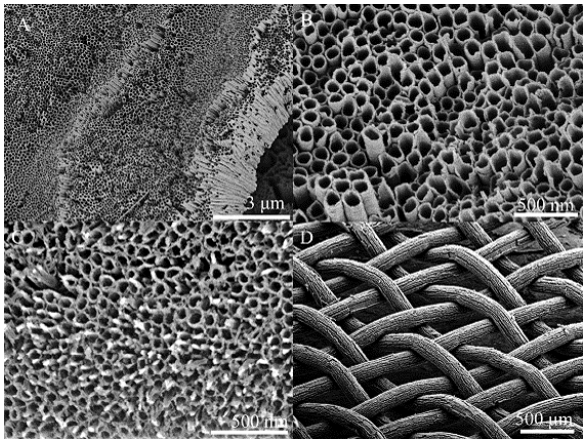

Fig.1 FESEM images of (A), (B) TTA-m and (C) TTA-m loaded with Pt as well as SEM image of (D) TTA-m loaded with Pt (anodization duration: 90 min; annealing temperature: 450 °C; content of Pt: 1.6 μmol·m^{-2}).

Fig. 1 shows the SEM image and the FESEM images of the samples. As can be seen from Fig 1A and 1B, the nanotubes arrays are fabricated on the Ti mesh via anodization followed by annealing. The as-prepared nanotubes arrays are composed of uniform and well-aligned nanotubes with an internal diameter of approximate 100 nm and a wall thickness of approximate 12 nm and an average length of 18 μm. Moreover, no other secondary nanostructures can be found at the mouths of nanotubes. Similarly, the FESEM image of the nanotubes arrays with Pt (Fig. 1C) shows few differences in the morphology of the nanotubes arrays after modification of Pt, except that there exist some bright secondary nanostructures at the mouths of nanotubes. The Pt-rich areas on the TiO_2 surface will exhibit relatively brighter images because Pt atom is heavier than Ti atom. Hence, it is reasonable to assume that the bright structures are the Pt nanoparticles on the TiO_2 nanotubes arrays. In addition, the SEM image taken at low magnification (Fig. 1D) shows that the nanotubes arrays loaded with Pt are fabricated on both longitudinal and horizontal wires in the Ti mesh. The distribution of the nanotubes is homogeneous and the coverage is very high (~100%). Analogously, from the TEM images (Fig. 2), we can observe no difference in the morphology of the nanotubes due to introduction of Pt. In addition, we also find from the TEM image of the TiO_2 nanotubes loaded with Pt (Fig. 2C) that some black nanoparticles are homogeneously distributed on the walls of the TiO_2 nanotubes. The HRTEM image (Fig. 2D) shows that there exist some lattice fringes in the black area on the walls of the TiO_2 nanotubes. The spacing between two conjoint planes is about 0.203 nm, corresponding to the (200) plane of Pt (JCPDS 04-0802).[29] These results indicate that the nanotubes arrays with Pt can be prepared successfully according to the procedure described above.

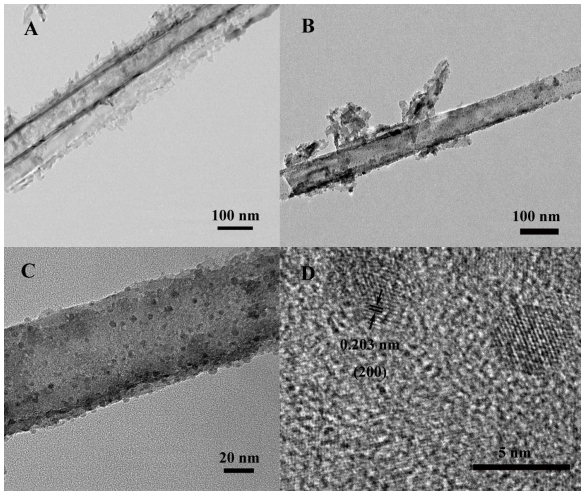

Fig.2 TEM images of (A) TiO_2 nanotube from TTA-m, (B), (C) TiO_2 nanotube from TTA-m loaded with Pt and (D) HRTEM image of TiO_2 nanotube from TTA-m loaded with Pt (anodization duration: 90 min; annealing temperature: 450 °C; content of Pt: 1.6 μmol·m^{-2}).

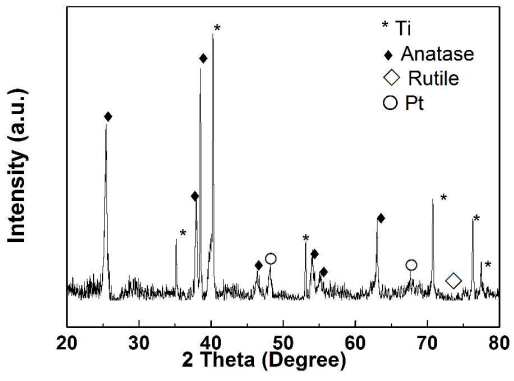

Fig.3 XRD pattern of TTA-m loaded with Pt (anodization duration: 90 min; annealing temperature: 450 °C; content of Pt: 1.6 μmol·m^{-2}).

RSC Advances Accepted Manuscript

Fig.3 shows the XRD pattern of TTA-m loaded with Pt (1.6 μmol·m^{-2}). From Fig. 3, it can be found that there exist five obvious diffraction peaks at 2θ=25.3°, 36.9, 48.0°, 53.9° and 55.1°, corresponding to (101), (103), (200), (105) and (211) planes of anatase TiO_2 (JCPDS 21-1272), respectively.[30] And two small peaks at 2θ= 46.2° and 67.5°, corresponding to (200) and (220) planes of Pt (JCPDS 04-0802),[29] can also be observed. Besides, a weak peak appears at 74.4°, corresponding to (320) plane of rutile TiO_2 (JCPDS 21-1276).[31] These results indicate that the crystallization of the as-prepared TiO_2 nanotubes arrays is anatase phase containing rutile. And Pt is deposited on the nanotubes arrays.

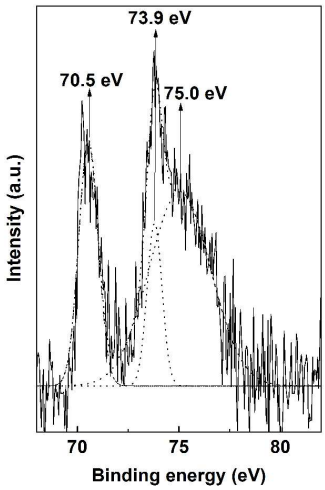

Fig.4 High-resolution XPS spectrum (solid line) of Pt 4f of TTA-m loaded with Pt, and curve-fitting analysis (dot lines) of states of Pt (anodization duration: 90 min; annealing temperature: 450 °C; content of Pt: 1.6 μmol·m^{-2}).

Fig. 4 shows the high-resolution XPS spectrum of Pt 4f. of TTA-m loaded with Pt (1.6 μmol·m^{-2}). It can be observed from Fig. 4 that there exist two broad peaks around 70.3 eV and 73.8 eV, respectively. The broad peak around 73.8 eV with a shoulder peak can be fitted by two peaks at 73.9 eV and 75.0 eV. The broad peak around 70.3 eV can be fitted by one peak at 70.5 eV. The peaks at 70.5 eV and 75.0 eV may be assigned to the Pt 4f7/2 peak and the Pt 4f5/2 peak of Pt^0,[32-34] while the peak at 73.9 eV should be attributed to Pt^{2+} species in PtO.[32] Compared with the characteristic Pt 4f7/2 peak (70.5-70.7 eV),[35] the Pt 4f7/2 binding energy observed is lower value. This phenomenon may be ascribed to a local increase of the electron density on Pt.[36] Hence, it can be deduced that there exists some strong interaction between TiO_2 nanotubes and Pt. And the Pt particles loaded are electron-rich,[34] which is favorable to the photocatalytic H_2 evolution. Moreover, the obvious peak at 73.9 eV indicates that PtO is formed during the preparation of TTA-m loaded with Pt. One possible explanation is that the surface energy of the Pt nanoparticles loaded on the TiO_2 nanotubes is high, so that a fraction of Pt is oxidized to PtO during calcination. However, the diffraction peaks of PtO cannot be found from Fig.3, suggesting that a thimbleful of Pt is oxidized. Combined with the results of SEM and XRD, it can be concluded that TTA-m loaded with Pt is successfully obtained. After calcination, Pt loaded is partially enveloped by a shell of PtO.

The Brunauer-Emmett-Teller (BET) measurement demonstrates that TTA-m loaded with Pt possesses considerable surface area. The apparent specific surface area of TTA-m loaded with Pt is 7.3 $m^2 \cdot g^{-1}$. Because the quality of the TiO_2 nanotubes arrays loaded with Pt accounts for only five percent of the total quality of sample, it can be deduced that the TiO_2 nanotubes arrays fabricated on Ti meshes actually possess relatively large surface area, which is comparable with that of P25 powder (50 $m^2 \cdot g^{-1}$).[37] These results indicate that TTA-m loaded with Pt may exhibit satisfactory photocatalytic activity for the H_2 evolution from water.

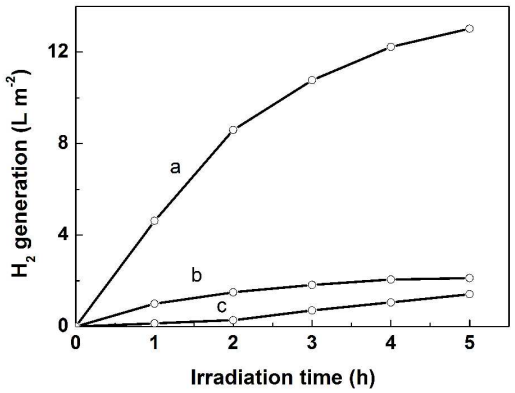

Fig.5 Irradiation time dependence of the amount of H_2 evolved from tri-ethanolamine aqueous solution over TTA-m loaded with Pt (a), the Pt-modified TiO_2 nanotubes arrays fabricated on Ti foils (b) and TTA-m (c) (irradiation area: 7.0 cm^2; anodization duration: 90 min; annealing temperature: 450 °C; content of Pt: 1.6 μmol·m^{-2}; tri-ethanolamine aqueous solution: 100 mL, 1 mol·L^{-1}; flow velocity: 25 mL·min^{-1}).

Fig. 5 shows the time-courses of H_2 evolution over TTA-m loaded with Pt, TTA-m or the Pt-modified TiO_2 nanotubes arrays fabricated on Ti foils under UV irradiation. As can be seen from Fig. 5, TTA-m loaded with Pt is an efficient photocatalyst which can be used in a continuous flow system for H_2 evolution. During the first hour of irradiation, the rate of H_2 evolution is up to 4.6 $L \cdot m^{-2}\ h^{-1}$. And the hydrogen production rate is almost constant in the first two hours, and then gradually decreases. The SEM image of the photocatalyst used (supplementary Fig. S1) shows that TTA-m possesses satisfactory stability. The morphology of nanotubes arrays is steady during the photocatalytic process. Therefore, this gradually decreases may be ascribed to the back reaction of H_2 on the surface of photocatalyst rather than the destruction of the TiO_2 nanotubes arrays. However, the rate of 1.2 $L \cdot m^{-2}\ h^{-1}$ can be still preserved after irradiated for 5 h. In contrast, TTA can hardly display photocatalytic activity for H_2 evolution from water. During the first hour of irradiation, only a rate of H_2 evolution of 0.14 $L \cdot m^{-2}\ h^{-1}$ can be achieved. This phenomenon indicates that Pt plays an important role in the photocatalytic process. Moreover, it can be also found from Fig. 5 that the photocatalytic activity of TTA-m loaded with Pt is much higher than that of the Pt-modified TiO_2 nanotubes arrays fabricated on

RSC Advances Accepted Manuscript

This journal is © The Royal Society of Chemistry [year]

Ti foils. The rate of H_2 evolution increases by a factor of 5 when the TiO_2 nanotube arrays are fabricated on metallic Ti meshes. This result suggests that Ti meshes are more suitable than Ti foils when they are applied in the immobilization of photocatalyst as substrates. On Ti meshes, the TiO_2 nanotubes arrays will reach their full potential in the photocatalytic process. In order to further demonstrate the excellent features of TTA-m loaded with Pt, the photocatalytic activity of the Ti meshes coated with P25 was explored and compared with that of TTA-m loaded with Pt. As expected, TTA-m loaded with Pt exhibits much higher photocatalytic activity in comparison with that of the Ti meshes coated with P25 (2.6 $L \cdot m^{-2} h^{-1}$). Besides, our control experimental results show that the TiO_2 nanotubes and the TiO_2 hollow microspheres only exhibit very low photocatalytic activities for H_2 evolution after immobilized on the solid substrates. The H_2 evolution rate over the TiO_2 nanotubes immobilized is only 0.47 $L \cdot m^{-2} h^{-1}$ while the rate over the TiO_2 hollow microspheres immobilized is 0.60 $L \cdot m^{-2} h^{-1}$. Therefore, it can be concluded that TTA-m loaded with Pt possesses superior photocatalytic activity and matches well with the continuous flow system, implying that TTA-m would have a broad application prospect in the immobilization of photocatalyst.

Based on the results above, a possible mechanism is suggested as follows. At first, when the TiO_2 nanotubes arrays is under irradiation, the electrons are excited from the valence band to the conduction band. And then the excited electrons transfer to Pt particles and are trapped efficiently due to the Schottky barrier between Pt and TiO_2. Consequently, water molecules are reduced into H_2 by the photogenerated electrons on Pt, and the holes are consumed irreversibly by tri-ethanolamine. Herein, Pt particles loaded act as charge transferring sites and/or active sites in the photocatalytic process. The higher photocatalytic activity of TTA-m loaded with Pt in comparison with that of the Pt-modified TiO_2 nanotubes arrays fabricated on Ti foils may be ascribed to two causes. (1) The apparent specific surface area of TTA-m loaded with Pt is 7.3 $m^2 \cdot g^{-1}$, while the apparent specific surface area of the Pt-modified TiO_2 nanotubes arrays fabricated on Ti foils is 2.1 $m^2 \cdot g^{-1}$. The larger surface area of TTA-m loaded with Pt implies the availability of more active sites, which improves the photocatalytic H_2 evolution. Here, the large surface area of TTA-m loaded with Pt may be ascribed to its 3-D hierarchical nanostructure. (2) The 3-D hierarchical nanostructure of TTA-m loaded with Pt would lead to enhancement of light harvesting because of light scattering. In order to confirm our assumption, the UV-vis spectra of TTA-m loaded with Pt and the Pt-modified TiO_2 nanotubes arrays fabricated on Ti foils were measured, respectively (Fig. 6). It can be observed from the UV spectrum of TTA-m loaded with Pt (Fig. 6a) that there exists a strong absorption band with an edge at approximate 410 nm, corresponding to the band gap transition of TiO_2 nanotubes arrays. In addition, compared with the Pt-modified TiO_2 nanotubes arrays fabricated on Ti foils, TTA-m loaded with Pt possesses much stronger capacity of light absorption in ultraviolet region, which confirms our assumption. However, in visible region, the absorption of the Pt-modified TiO_2 nanotubes arrays fabricated on Ti foils is relatively stronger. One possible explanation is that the 3-D nanotubes arrays on Ti meshes are fabricated on the curved surface of Ti wires while the 2-D TiO_2 nanotubes arrays on Ti foils are fabricated on the planar substrates. Thus, the 2-D TiO_2 nanotubes arrays fabricated on Ti foils may be more compact than the 3-D nanotubes arrays fabricated on Ti wires in the Ti mesh. When Pt is electrodeposited on the nanotubes arrays, the dispersion of Pt particles in the nanotubes layer on Ti meshes is more homogeneous than that on Ti foils. As a result, the Pt-modified TiO_2 nanotubes arrays fabricated on Ti foils shows stronger absorption in visible region. Moreover, the relatively homogeneous dispersion of Pt particles on Ti meshes may be another factor which causes the high photocatalytic activity of TTA-m loaded with Pt.

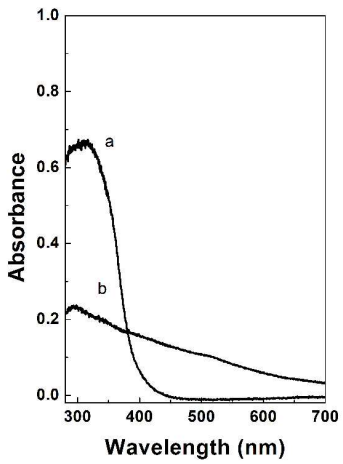

Fig. 6 UV-vis spectra of TTA-m loaded with Pt (a) and the Pt-modified TiO_2 nanotubes arrays fabricated on Ti foils (b) (anodization duration: 90 min; annealing temperature: 450 °C; content of Pt: 1.6 $\mu mol \cdot m^{-2}$).

Fig. 7 shows the effect of flow velocity of tri-ethanolamine solution on the photocatalytic hydrogen evolution over TTA-m loaded with Pt. It can be found that the rate of H_2 evolution is almost constant when the flow velocity of tri-ethanolamine solution increases from 8 $mL \cdot min^{-1}$ to 80 $mL \cdot min^{-1}$. This result indicates that TTA-m loaded with Pt possesses satisfactory mechanical stability, and can be applied in a wide flow velocity range. On the other hand, when the flow velocities of tri-ethanolamine solution are 8 $mL \cdot min^{-1}$ and 80 $mL \cdot min^{-1}$, the corresponding rates of H_2 evolution can be regarded as the hourly output of H_2 from the static reaction systems whose volumes are 480 mL and 4800 mL, respectively. Thus it can be seen that TTA-m loaded with Pt is an efficient photocatalyst for photocatalytic H_2 evolution from water. And the rate of H_2 evolution over TTA-m loaded with Pt may be controlled by the surface reactions rather than the diffusion and adsorption of reactants and products.

Fig. 8 shows the effect of anodization duration on the photocatalytic hydrogen evolution over TTA-m loaded with Pt. As can be seen from Fig. 8, the rate of H_2 evolution gradually increases with the anodization duration increasing from 15 min to 90 min, and thereafter begins to decrease with increasing the anodization duration. The optimal anodization duration is 90 min. The experimental results reported previously indicate that the TiO_2 nanotube length increases almost linearly during first 10 h

RSC Advances Accepted Manuscript

anodization in glycerol-based electrolytes while difference in tube diameter can hardly be observed.[38] From these results, it can be inferred that the length of the TiO_2 nanotubes on Ti meshes will become longer and longer with increasing anodization duration while the diameter of the TiO_2 nanotubes is almost constant. As a result, the surface area of TiO_2 nanotubes arrays, the aspect ratio of TiO_2 nanotubes and the content of TiO_2 will all increase when the anodization duration is prolonged, which leads to the enhancement of the photocatalytic activity of TTA-m loaded with Pt. However, the mechanical stability of TTA-m loaded with Pt will decreases when the TiO_2 nanotubes become longer. Under shear of flow solution, long TiO_2 nanotubes on Ti meshes may be broken more easily in comparison with short TiO_2 nanotubes. Therefore, the rate of H_2 evolution gradually decreases with the anodization duration increasing from 90 min to 240 min.

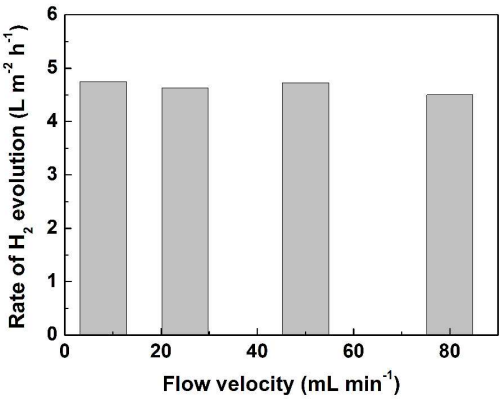

Fig. 7 Effect of the flow velocity on the hydrogen production rate over TTA-m loaded with Pt (irradiation area: 7.0 cm^2; anodization duration: 90 min; annealing temperature: 450 °C; content of Pt: 1.6 μmol·m^{-2}; tri-ethanolamine aqueous solution: 100 mL, 1 mol·L^{-1}).

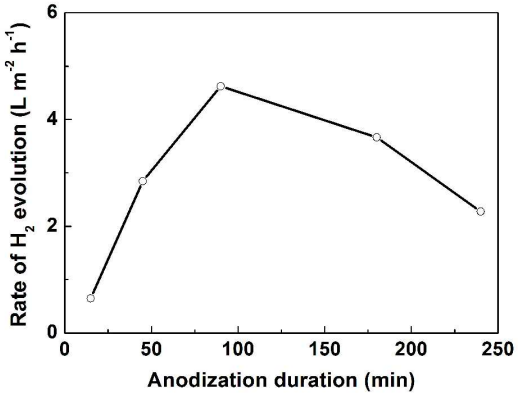

Fig. 8 Effect of the anodization duration on the hydrogen production rate over TTA-m loaded with Pt (irradiation area: 7.0 cm^2; annealing temperature: 450 °C; content of Pt: 1.6 μmol·m^{-2}; tri-ethanolamine aqueous solution: 100 mL, 1 mol·L^{-1}; flow velocity: 25 mL·min^{-1}).

Fig. 9 shows the effect of annealing temperature on the photocatalytic hydrogen evolution over TTA-m loaded with Pt. It can be observed that the photocatalytic activity of TTA-m loaded with Pt increases gradually when the annealing temperature increases from 200 °C to 450 °C. If the annealing temperature further increases, the photocatalytic activity of TTA-m loaded with Pt decreases. It is well known that the crystallinity of samples will be enhanced with increasing annealing temperature. There exists less lattice defects in the samples with high crystallinity, which will facilitate the electron transport to active sites. As a result, the photocatalytic activity of TTA-m loaded with Pt is enhanced with the annealing temperature increasing from 200 °C to 450 °C. However, when the annealing temperature increases from 450 °C to 800 °C, the crystalline phase of TTA-m may be transformed from anatase to rutile. Thus, the photocatalytic activity of TTA-m loaded with Pt annealed at 800 °C is lower than that of the sample annealed at 450 °C.

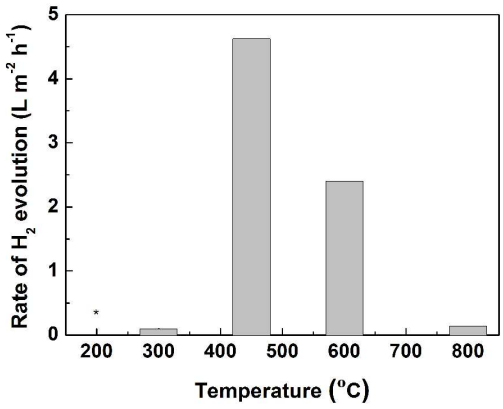

Fig. 9 Effect of the annealing temperature on the hydrogen production rate over TTA-m loaded with Pt (irradiation area: 7.0 cm^2; anodization duration: 90 min; content of Pt: 1.6 μmol·m^{-2}; tri-ethanolamine aqueous solution: 100 mL, 1 mol·L^{-1}; flow velocity: 25 mL·min^{-1}, "*" means no hydrogen evolution).

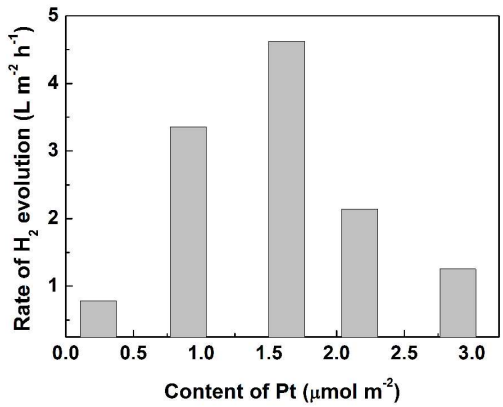

Fig.10 Effect of the content of Pt on the hydrogen production rate over TTA-m loaded with Pt (irradiation area: 7.0 cm^2; anodization duration: 90 min; annealing temperature: 450 °C; tri-ethanolamine aqueous solution: 100 mL, 1 mol·L^{-1}; flow velocity: 25 mL·min^{-1}).

RSC Advances Accepted Manuscript

This journal is © The Royal Society of Chemistry [year]

Fig 10 shows the effect of content of Pt on the photocatalytic hydrogen evolution over TTA-m loaded with Pt. As can be seen from Fig. 10, the rate of H_2 evolution gradually increases with increasing the content of Pt from 0.24 to 1.63 μmol·m^{-2}, and then begins to decrease with increasing the content of Pt. One possible explanation is that when the content of Pt is less than the optimal content, the number of Pt particles, i.e. active sites, would increase with increasing the content of Pt, resulting in the improvement of the photocatalytic activity. However, if the content of Pt is more than the optimal content, the efficient contact between Pt and TiO_2 nanotubes may decrease due to enlargement of Pt particles, which is unfavorable to the electron transfer from the conduction band of TiO_2 to Pt.[39] Moreover, another possible explanation is that the Pt particles may act as the recombination centers of electron-hole pairs when excess Pt is deposited on the TiO_2 nanotubes.[40] As a result, excessively high content of Pt will cause the decrease of the photocatalytic activity of TTA-m loaded with Pt.

Conclusions

In conclusion, TiO_2 nanotubes arrays were successfully fabricated on metallic Ti meshes and decorated with Pt using anodic oxidation followed by electrodeposition. TTA-m loaded with Pt is an efficient and promising photocatalyst for the photocatalytic H_2 evolution in a continuous flow system. Ti meshes are more suitable than Ti foils when they are applied in the immobilization of photocatalyst as substrates. Herein, the 3-D hierarchical nanostructure plays an important role. This work provides us with new possibility for designing an efficient photocatalyst which can be used in a continuous flow system. Further efforts are currently being undertaken.

Acknowledgements

This work was financially supported by the Key Project of Science and Technology Innovation of Shanghai Education Commission (No. 13ZZ135), the Open Project of State Key Laboratory of Supramolecular Structure and Materials (No. sklssm201424) and the National Natural Science Foundation of China (No. 21301118).

Notes and references

[a] *School of Chemical and Environmental Engineering, Shanghai Institute of Technology, 100 Haiquan Road, Shanghai, 201418, China. Fax and Tel: 86 21 60873061; E-mail: kangsz@sit.edu.cn, mujin@sit.edu.cn*
[b] *School of Chemistry and Molecular Engineering, East China University of Science and Technology, 130 Meilong Road, Shanghai 200237, China*

† Electronic Supplementary Information (ESI) available: [details of any supplementary information available should be included here]. See DOI: 10.1039/b000000x/

1 A. Kruth, S. Hansen, T. Beweries, V. Brser, and K. Weltmann, *Chem. Sus. Chem.,* 2013, **6**, 152.
2 M. P. Languer, F. R. Scheffer, A. F. Feil, D. L. Baptista, P. Migowski, G. J. Machado, D. P. de Moraes, J. Dupont, S. R. Teixeira, and D. E. Weibel, *Int. J. Hydrogen Energy*., 2013, **38**, 14440.
3 Z. Li, Y. Chen, Y. Du, X. Wang, P. Yang, and J. Zheng, *Int. J. Hydrogen Energy.,* 2012, **37**, 4880.
4 Y. Chen, Z. Mou, S. Yin, H. Huang, P. Yang, X. Wang, and Y. Du, *Mater. Lett.,* 2013, **107**, 31.
5 H.-B. He, M. Chang, A.-P. Chen, L. Ma, H.-J. Dong, C.-Z. Li, and N. Anode, *Chin. J. Inorg. Chem.,* 2012, **28**, 2097.
6 J. Boucle, and J. Ackermann, *Polym. Int.,* 2012, **61**, 355.
7 L. Giodano, and G. Pacchion, *Acc. Chem. Res.,* 2011, **44**, 1244.
8 A. Kubacka, M. Fernandez-Garcia, and G. Colon, *Chem. Rev,*. 2012, **112**, 1555.
9 D. V. Bavykin, J. M. Friedrich, and F. C. Walsh, *Adv. Mater.,* 2006, **18,** 2807.
10 H. Li, W. Zhang, and W. Pan, *J. Am. Ceram. Soc,*. 2011, **94,** 3184.
11 S. Hoang, S. Guo, and C. B. Mullins, *J. Phys. Chem. C.,* 2012, **116**, 23283.
12 D. Wang, and L. Liu, *Chem. Mater.,* 2010, **22**, 6656.
13 J.-K. Oh, J.-K. Lee, H.-S. Kim, S.-B. Han, and K.-W. Park, *Chem. Mater.,* 2010, **22**, 1114.
14 M. Arabatzis, S. Antonaraki, T. Stergiopoulos, A. Hiskia, E. Papaconstantinou, M. C. Bernard, and P. *Falaras, J. Photochem. Photobiol. A,* 2002, **149**, 237.
15 A. Pozio, M. Carewska, F. Mura, R. D'Amato, M. Falconieri, M. De Francesco, and G. B. Appetecchi, *J. Power Sources*, 2014, **247,** 883.
16 Z. Q. Bao, H. X. Xie, J. Rao, L. Chen, Y. Wei, H. F. Li, and X. F. Zhou, *Mater. Lett.,* 2014, **124**, 158.
17 Y. Hou, X. Li, Q. Zhao, X. Quan, and G. Chen, *Environ. Sci. Technol.,* 2010, **44**, 5098.
18 L. Tsui, J. Huang, M. Sabat, and G. Zangari, *ACS Sustainable Chem. Eng.,* 2014, 2, 2097-2101.
19 Y. Lai, J. Gong, and C. Lin. *Int. J. Hydrogen Energy,* 2012, **37**, 6438.
20 Y. Sun, G. Wang, and K. Yan, *Int. J. Hydrogen Energy,* 2011, **36,** 15502.
21 Z. Jiao, Y. Zhang, T. Chen, Q. Dong, G. Lu, and Y. Bi, *Chem. Eur. J.,* 2014, **20**, 2654.
22 M. Ye, J. Gong, Y. Lai, C. Lin, and Z. Lin, *J. Am. Chem. Soc.,* 2012, **134**, 15720.
23 S. K. Mohapatra, M. Misra, V. K. Mahajan, and K. S. Raja, *J. Phys. Chem. C,* 2007, **111**, 8677.
24 Y. Sun, K. Yan, G. Wang, W. Guo, and T. Ma, *J. Phys. Chem. C,* 2011, **115**, 12844-12849.
25 N. Liu, C. Schneider, D. Freitag, M. Hartmann, U. Venkatesan, J. Muller, E. Spiecker, and P. Schmuki, *Nano Lett*., 2014, **14**, 3309.
26 Z. Liu, Q. Zhang, T. Zhao, J. Zhai, and L. Jiang, *J. Mater. Chem.,* 2011, **21**, 10354.
27 Z. Zhang, X. Yang, M. N. Hedhili, E. Ahmed, L. Shi, and P. Wang, *ACS Appl. Mater. Interfaces,* 2014, **6,** 691.
28 L Xing, J. Jia, Y. Wang, B. Zhang, and S. Dong, *Int. J. Hydrogen Energy,* 2010, **35**, 12169.
29 Y. Luo, S. K. Lee, H. Hofmeister, M. Steinhart, and U. Go1sele, *Nano Lett.,* 2004, 4, 143.
30 Y. Du, Q. Feng, C. Chen, Y. Tanaka, and X. Yang, *ACS Appl. Mater. Interfaces,* 2014, **6**, 16007.
31 Y. Zou, S.-Z. Kang, X. Li, L. Qin, and J. Mu, *Int. J. Hydrogen Energy*, 2014. **39**, 15403.
32 R. Siburian, and J. Nakamura, *J. Phys. Chem. C*, 2012, **116**, 22947.
33 B.-H. Chen, and J, M. White, *J. Phys. Chem.,* 1982, **86**, 3534.
34 J. Ohyama, A. Yamamoto, K. Teramura, T. Shishido, and T. Tanaka, *ACS Catal.*. 2011, **1**, 187.
35 P. Concepcion, A. Corma, J. Silvestre-Albero, V. Franco, and J. Y. Chane-Ching, *J. Am. Chem. Soc.,* 2004, **126**, 5523.
36 A. Lewera, L. Timperman, A. Roguska, and N. Alonso-Vante, *J. Phys. Chem. C,* 2011, **115**, 20153.
37 J. Yu, X. Zhao, J. Du, and W. Chen, *J. Sol-Gel Sci. Technol*., 2000, **17**, 163.
38 J. M. Macak, and P. Schmuki, *Electrochim. Acta*, 2006, **52**, 1258.
39 S.-Z. Kang, L. L. Chen, X. Q. Li, and J. Mu, *Appl. Surf. Sci.,* 2012, **258**, 6029.
40 W.-C. Lin, W.-D. Yang, I.-L. Huang, T.-S. Wu, and Z.-J. Chung, *Energy Fuels*, 2009, **23**, 2192.

RSC Advances Accepted Manuscript